

Differentiable Quantum Architecture Search in Quantum-Enhanced Neural Network Parameter Generation

Samuel Yen-Chi Chen^{*††}, Chen-Yu Liu^{†xi}, Kuan-Cheng Chen^{‡§xii},
Wei-Jia Huang^{¶xiii}, Yen-Jui Chang^{||**xiv}, Wei-Hao Huang^{‡‡x}

^{*}Wells Fargo, New York, NY, USA

[†]Graduate Institute of Applied Physics, National Taiwan University, Taipei, Taiwan

[‡]Department of Electrical and Electronic Engineering, Imperial College London, London, UK

[§]Centre for Quantum Engineering, Science and Technology (QuEST), Imperial College London, London, UK

[¶]Hon Hai (Foxconn) Research Institute, Taipei, Taiwan

^{||}Quantum Information Center, Chung Yuan Christian University, Taoyuan City, Taiwan

^{**}Master Program in Intelligent Computing and Big Data, Chung Yuan Christian University, Taoyuan City, Taiwan

^{‡‡}Jij inc., Tokyo, Japan

Email: ^{††} yen-chi.chen@wellsfargo.com, ^x w.huang@j-ij.com, ^{xi} d10245003@g.ntu.edu.tw,
^{xii} kuan-cheng.chen17@imperial.ac.uk, ^{xiii} wei-jia.huang@foxconn.com, ^{xiv} aceest@cycu.edu.tw

Abstract—The rapid advancements in quantum computing (QC) and machine learning (ML) have led to the emergence of quantum machine learning (QML), which integrates the strengths of both fields. Among QML approaches, variational quantum circuits (VQCs), also known as quantum neural networks (QNNs), have shown promise both empirically and theoretically. However, their broader adoption is hindered by reliance on quantum hardware during inference. Hardware imperfections and limited access to quantum devices pose practical challenges. To address this, the Quantum-Train (QT) framework leverages the exponential scaling of quantum amplitudes to generate classical neural network parameters, enabling inference without quantum hardware and achieving significant parameter compression. Yet, designing effective quantum circuit architectures for such quantum-enhanced neural networks remains non-trivial and often requires expertise in quantum information science. In this paper, we propose an automated solution using differentiable optimization. Our method jointly optimizes both conventional circuit parameters and architectural parameters in an end-to-end manner via automatic differentiation. We evaluate the proposed framework on classification, time-series prediction, and reinforcement learning tasks. Simulation results show that our method matches or outperforms manually designed QNN architectures. This work offers a scalable and automated pathway for designing QNNs that can generate classical neural network parameters across diverse applications.

Index Terms—Quantum Machine Learning, Quantum Neural Networks, Variational Quantum Circuits, Model Compression, Learning to Learn

I. INTRODUCTION

Quantum computing (QC) and quantum machine learning (QML) are rapidly advancing frontiers that promise to re-

shape computational approaches across a wide range of fields [1], [2]. Among various QML strategies, variational quantum algorithms (VQAs) [3], [4] have emerged as a prominent framework designed to operate on noisy intermediate-scale quantum (NISQ) hardware. Recent theoretical analyses have highlighted potential advantages of VQAs over classical machine learning under specific conditions, such as in terms of model expressivity and generalization behavior [5]–[8]. These capabilities have stimulated a growing body of work applying QML techniques to diverse tasks, including classification [9]–[17], reinforcement learning [18]–[28], time-series modeling [28]–[32], and natural language processing [33]–[37].

Despite recent progress, conventional QML approaches continue to face major obstacles—most notably, the difficulty of encoding large-scale classical data into quantum circuits. Common strategies such as gate-angle encoding and amplitude encoding are fundamentally constrained by the limited number of available qubits and the short coherence times of near-term quantum hardware, posing critical barriers to scalability and real-world deployment. In addition, the inference stage of QML models typically relies on access to quantum processors—often through cloud-based services—where hybrid quantum-classical computations are executed sequentially across circuit layers. This architectural dependence introduces latency and computational inefficiencies, especially in time-critical scenarios such as autonomous control or online decision-making.

To address these limitations, a hybrid architecture known as Quantum-Train (QT) has been proposed [31], [38]–[49]. The core idea behind QT is to shift the role of quantum computation from data processing to parameter generation. Specifically, a quantum neural network (QNN) is trained to output the weights of a classical neural network, allowing clas-

The views expressed in this article are those of the authors and do not represent the views of Wells Fargo. This article is for informational purposes only. Nothing contained in this article should be construed as investment advice. Wells Fargo makes no express or implied warranties and expressly disclaims all legal, tax, and accounting implications related to this article.

sical data to be processed entirely on a classical architecture. This design eliminates the need for quantum data encoding and removes dependency on quantum hardware during inference, resulting in a fully classical model after training—well-suited for deployment in near-term applications.

However, existing QT frameworks still rely on manually crafted QNN architectures, often requiring expert-level domain knowledge and trial-and-error validation. This design bottleneck presents a steep barrier for widespread adoption outside the quantum machine learning community. To overcome this challenge, we propose Quantum-Train with Differentiable Quantum Architecture Search (DiffQAS-QT)—a novel framework that automates the discovery of high-performing QNN architectures specifically designed to generate classical neural network parameters for downstream learning tasks.

In this study, we demonstrate the versatility and effectiveness of DiffQAS-QT across a diverse set of machine learning tasks, including image classification, time-series forecasting, and reinforcement learning. Our experiments show that DiffQAS-QT delivers strong performance on MNIST classification, accurate rollout prediction in QT-enhanced LSTM models for temporal data, and robust policy learning in A3C-based QT-RL agents navigating MiniGrid environments. Notably, the proposed framework achieves not only high predictive accuracy but also superior training stability across modalities. These results suggest that DiffQAS-QT offers a promising direction for automating QNN design and advancing hybrid quantum-classical learning in practical settings.

II. RELATED WORKS

Quantum-Train (QT) is a hybrid framework in which a quantum neural network (QNN) is employed to generate the parameters—such as weights and biases—of a classical neural network [38], [39], [48]. By shifting the role of quantum computation from data processing to parameter synthesis, QT provides an alternative approach to hybrid learning that avoids the costly data encoding bottleneck common in many QML systems.

Since its initial formulation, the QT framework has been extended to a wide range of machine learning domains. In image classification, QT-based architectures have been applied to build compact yet expressive visual models [39], [42], [43]. For time-series forecasting, QT-enhanced recurrent networks (QT-LSTM) and fast weight programmers have been explored for modeling temporal dynamics in both centralized and federated settings [31], [45], [47]. The framework has also been adopted for federated learning scenarios to provide privacy-preserving features [41], [45], enabling decentralized training of quantum-informed models without direct sharing of raw data. In addition, recent works have applied QT to natural language processing tasks [44], [49], as well as to reinforcement learning, where QT-generated policies are trained within quantum-classical agent architectures [40], [46]. While numerous QML architectures such as the QNN used in QT have demonstrated promising empirical performance, a major barrier to their widespread adoption in practical

applications lies in the significant expertise required to design high-performing quantum circuits. In particular, constructing effective QNN architectures often demands deep domain knowledge in quantum information science, limiting accessibility to a broader machine learning audience. *Quantum architecture search* (QAS) has emerged as a promising research direction aimed at alleviating this bottleneck. The goal of QAS is to automatically generate efficient quantum circuit architectures for target tasks—such as quantum state preparation or QML model training—with minimal or no manual intervention from the user [50]. A range of methods have been proposed to tackle this challenge. One popular line of work frames circuit construction as a sequential decision-making process, making reinforcement learning (RL) a natural candidate for QAS [51]–[54]. While RL-based approaches are theoretically universal solvers, they face several practical challenges, including the exploration–exploitation trade-off, sensitivity to optimizer hyperparameters, and high sample complexity. To address some of these issues, evolutionary QAS methods have been introduced [55], [56]. These methods encode quantum circuits into genetic representations (e.g., chromosomes), and evolve a population \mathcal{P} of architectures through selection, crossover, and mutation over successive generations. Fitness scores—based on fidelity, QML task performance, or information-theoretic measures—guide the evolutionary process. A notable advantage of evolutionary QAS is its natural amenability to parallelization, allowing efficient deployment on high-performance computing (HPC) resources, particularly for batch evaluation of candidate circuits. Despite these advances, a fundamental limitation remains: both RL-based and evolutionary approaches operate in discrete search spaces, where the combinatorial explosion of candidate architectures can become prohibitive as the search space expands. Inspired by classical neural architecture search (NAS) [57], recent works propose differentiable QAS methods [58]–[61], where the architecture space is relaxed into a continuous domain using structural weights or parameterized distributions over candidate circuits. This relaxation enables gradient-based optimization over architecture parameters alongside circuit parameters in an end-to-end fashion.

In this work, we integrate differentiable QAS with the Quantum-Train (QT) framework. This combination enables us to explore a much larger architectural search space without suffering from the discrete sampling inefficiencies present in RL and evolutionary methods. Furthermore, it allows us to jointly optimize both the variational parameters within the quantum circuit and the architecture parameters controlling circuit structure, under a unified differentiable pipeline—ultimately enabling smooth, gradient-based training of quantum-generated classical models.

III. QUANTUM NEURAL NETWORKS

Variational Quantum Circuits (VQCs), also referred to as *parameterized quantum circuits* (PQCs), represent a widely studied class of quantum models characterized by their tunable gate parameters. In modern hybrid quantum–classical learning

paradigms, VQCs serve as the foundational building blocks for quantum neural networks (QNNs) [4], [9]. A growing body of theoretical work has shown that VQCs are capable of exhibiting specific forms of quantum advantage under appropriate conditions [5]–[7], underscoring their relevance to quantum machine learning applications. The standard design of a VQC

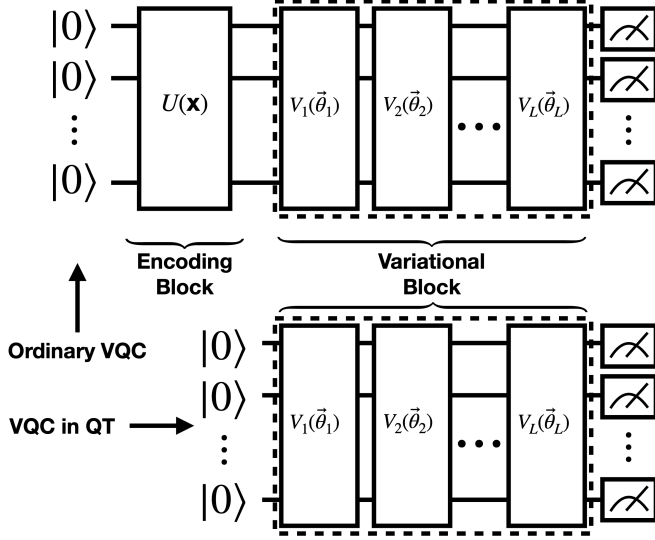


Fig. 1. **Comparison between standard VQC and VQC used in the Quantum-Train (QT) framework.** The upper circuit illustrates a conventional variational quantum circuit, which consists of an encoding block $U(\vec{x})$ for input-dependent state preparation, followed by a variational block composed of layered parametrized unitaries $\{V_\ell(\vec{\theta}_\ell)\}$. In contrast, the lower diagram shows the VQC design employed in QT, where the encoding circuit is omitted. By initializing directly from the ground state $|0\rangle^{\otimes n}$, the QT-based VQC reduces circuit depth and resource requirements, facilitating more efficient quantum execution.

comprises three principal stages: (1) an input encoding circuit, (2) a sequence of parameterized quantum layers forming the variational core, and (3) a final measurement process. As depicted in the upper section of Figure 1, the encoding circuit $U(\mathbf{x})$ transforms a classical input vector \mathbf{x} into a quantum state by acting on the initial all-zero qubit state $|0\rangle^{\otimes n}$, resulting in the embedded quantum state $|\Psi\rangle = U(\mathbf{x})|0\rangle^{\otimes n}$, where n is the number of qubits involved. Following the encoding stage, the quantum state is processed by a variational block—indicated by the dashed box—consisting of multiple layers $V_j(\vec{\theta}_j)$ of trainable unitaries. Each layer may incorporate entangling operations (e.g., CNOT gates) as well as single-qubit parameterized rotations such as R_x , R_y or R_z . The overall trainable module is denoted by $W(\Theta)$, defined as the ordered product:

$$W(\Theta) = V_L(\vec{\theta}_L)V_{L-1}(\vec{\theta}_{L-1})\cdots V_1(\vec{\theta}_1), \quad (1)$$

where L is the number of layers and $\Theta = \{\vec{\theta}_1, \dots, \vec{\theta}_L\}$ collects all learnable parameters. Each vector $\vec{\theta}_k$ contains rotation parameters for the k -th layer. In the context of the *Quantum-Train* (QT) framework, the VQC structure remains largely consistent with the conventional form, except for two

key differences. First, the encoding block $U(\mathbf{x})$ is omitted, meaning the circuit operates directly from the ground state $|0\rangle^{\otimes n}$, thereby reducing circuit depth and resource overhead. Second, the measurement strategy diverges from the standard approach: while traditional VQCs typically compute expectation values of fixed observables such as Pauli- Z , yielding output vectors of the form

$$\overrightarrow{f(\mathbf{x}; \Theta)} = (\langle \hat{Z}_1 \rangle, \dots, \langle \hat{Z}_n \rangle), \quad (2)$$

with each component given by

$$\langle \hat{Z}_k \rangle = \langle 0 | U^\dagger(\mathbf{x}) W^\dagger(\Theta) \hat{Z}_k W(\Theta) U(\mathbf{x}) | 0 \rangle, \quad (3)$$

the QT module instead retrieves the full distribution over all 2^n computational basis states (e.g., $|00\dots 0\rangle, \dots, |11\dots 1\rangle$). These measurement probabilities are subsequently utilized in downstream classical post-processing or model generation tasks.

IV. QUANTUM-TRAIN

Given a target classical model such as a deep neural network with p parameters, denoted $\kappa \in \mathbb{R}^p$, the Quantum-Train (QT) framework utilizes a quantum neural network (QNN) comprising $n_{qt} = \lceil \log_2 p \rceil$ qubits. This configuration defines a Hilbert space of dimension $2^{n_{qt}} \geq p$, enabling the generation of $2^{n_{qt}}$ measurement outcomes, each corresponding to a basis state $|\phi_i\rangle$, where $i \in 1, 2, \dots, 2^{n_{qt}}$. The associated probabilities are given by $|\langle \phi_i | \psi(\gamma) \rangle|^2 \in [0, 1]$, where $|\psi(\gamma)\rangle$ represents the QNN output state parameterized by γ . These probabilities are subsequently transformed into real-valued outputs via a classical mapping function \mathcal{M}_β , parameterized by β . Implemented as a multi-layer perceptron (MLP), \mathcal{M}_β takes both the basis state label $|\phi_i\rangle$ (written in binary representation with length n_{qt}) and its corresponding measurement probability as input to generate the classical model parameter κ_i :

$$\mathcal{M}_\beta(|\phi_i\rangle, |\langle \phi_i | \psi(\gamma) \rangle|^2) = \kappa_i, \quad \forall i \in 1, 2, \dots, p. \quad (4)$$

Consequently, training the classical model parameters κ entails joint optimization over the QNN parameters γ and the mapping function parameters β . Provided that both $|\psi(\gamma)\rangle$ and \mathcal{M}_β require only $O(\text{poly}(n_{qt}))$ parameters [3], [62], this approach yields an effective compression from p to $O(\text{polylog}(p))$ parameters. An overview of the QT mechanism is illustrated in Figure 2.

V. DIFFERENTIABLE QUANTUM ARCHITECTURE SEARCH

Building upon ideas from classical neural architecture search (NAS) [57] and recent developments in differentiable quantum architecture search (DiffQAS) [58], [60], our method begins by defining a set of candidate quantum subcircuits. Suppose we aim to construct a quantum circuit \mathcal{C} , composed of multiple modular components $\mathcal{S}_1, \mathcal{S}_2, \dots, \mathcal{S}_n$. Each sub-component \mathcal{S}_i can be instantiated by selecting from a set of predefined circuit structures \mathcal{B}_i , and the cardinality $|\mathcal{B}_i|$ determines the number of possible designs at that position. Consequently, the total design space for \mathcal{C} includes $N =$

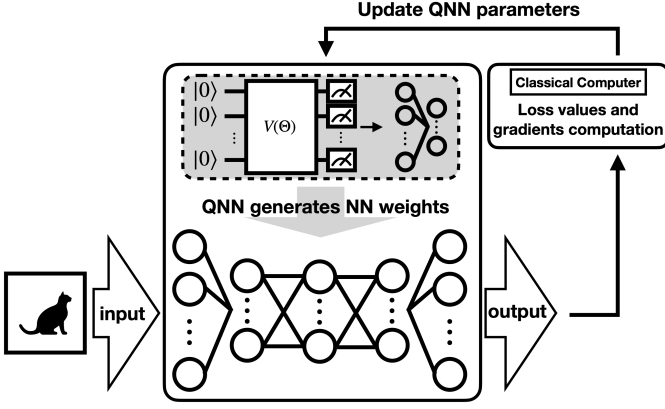


Fig. 2. Concept of Quantum-Train.

$|\mathcal{B}_1| \times |\mathcal{B}_2| \times \dots \times |\mathcal{B}_n|$ unique circuit configurations. For each candidate realization \mathcal{C}_j within this space, we assign a learnable structural weight w_j , where $j \in 1, \dots, N$. Each configuration \mathcal{C}_j is also associated with a distinct set of trainable quantum parameters θ_j . In a given machine learning task, some configurations may lead to well-performing models when trained, while others may prove ineffective. To integrate all possible candidates, we define an ensemble function f_C as a weighted combination over all N candidates:

$$f_C = \sum_{j=1}^N w_j f_{C_j} \quad (5)$$

where for brevity, we omit explicit references to the inputs \vec{x} and internal parameters θ_j . The ensemble output f_C is then evaluated using a task-specific loss function $\mathcal{L}(f_C)$. By leveraging automatic differentiation, we compute gradients with respect to the structural weights w_j , i.e., $\nabla_{w_j} \mathcal{L}(f_C)$, allowing standard gradient-based optimization techniques to update the weights efficiently. Within the DiffQAS framework, variational quantum circuits (VQCs) are constructed by selecting from a set of pre-defined ansatz candidates, as depicted in Figure 3. Unlike traditional QNNs, the Quantum-Train (QT) setting omits an explicit encoding circuit. Instead, the architecture is formed by choosing among three design dimensions: (1) whether to apply Hadamard gates at initialization to generate unbiased superpositions, (2) which entangling layer to use (two choices are provided), and (3) the type of rotation gates to be applied (R_x , R_y , or R_z). This results in $2 \times 2 \times 3 = 12$ total architecture candidates for a single-layer VQC or QNN, each assigned an individual weight w_j . To enhance expressiveness and accommodate more complex tasks, multiple ensemble layers can be stacked to build deeper quantum circuits. If M such layers are employed, the total number of structural weights increases to $N \times M$, reflecting the full space of configurable subcircuits across all layers. All structural weights across the depth of the circuit can be jointly optimized through differentiable programming techniques and standard optimizers. The overall concept of integrating Quantum-Train with DiffQAS is illustrated in Figure 4. Based on the set of allowed circuit components defined in Figure 3, we construct all 12 feasible circuit configurations. During each forward pass, all candidate cir-

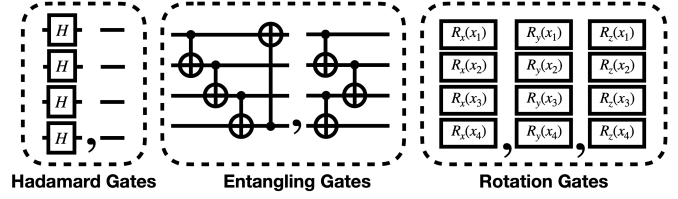


Fig. 3. Ansatzes of QNN/VQC considered in this work.

cuits—implemented as n -qubit QNNs—independently execute their quantum computations, each producing 2^n measurement probabilities corresponding to the computational basis states. These outputs are subsequently aggregated via a weighted summation governed by the trainable structural weights w_j , yielding the final ensemble output:

$$\text{output} = \sum w_j \text{VQC}_j(\theta^j) \quad (6)$$

where $\text{VQC}_j(\theta^j)$ denotes the output from the j -th variational

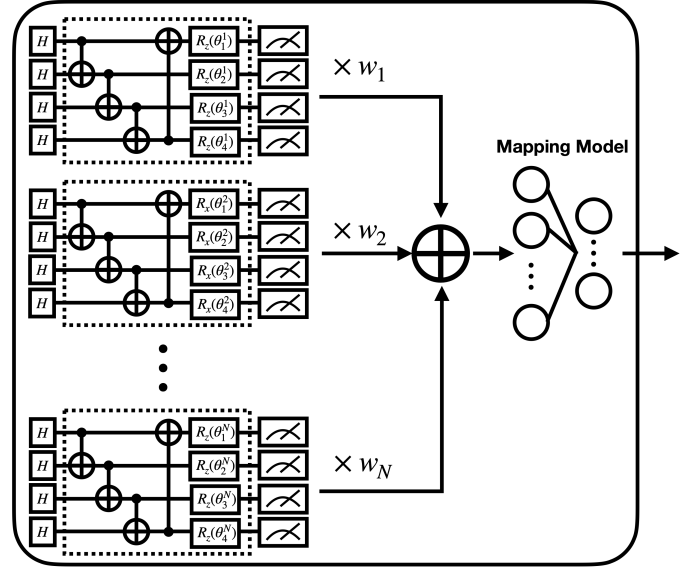


Fig. 4. Quantum-Train with DiffQAS

quantum circuit with its own parameter set θ^j . While assigning distinct parameter sets θ^j to each candidate architecture is theoretically permissible, doing so significantly increases the total number of trainable parameters. To mitigate this complexity, we adopt a shared parameter strategy in this study: a single parameter vector θ is used across all circuit variants. Accordingly, the ensemble output from the DiffQAS block simplifies to:

$$\text{output} = \sum w_j \text{VQC}_j(\theta). \quad (7)$$

VI. NUMERICAL RESULTS AND DISCUSSION

To assess the effectiveness of the proposed DiffQAS-QT framework, we conduct comprehensive evaluations across three categories of tasks: classification, time-series prediction, and reinforcement learning. Specifically, we benchmark performance on the MNIST and FashionMNIST datasets for classification; the Bessel function, damped simple harmonic motion (SHM), delayed quantum control, and NARMA-5/10

tasks for time-series prediction; and the MiniGrid-Empty environments (5×5 and 6×6) for reinforcement learning. In our comparisons, we include 12 baseline quantum neural network (QNN) configurations, detailed in Table I. For the entanglement strategy within the circuit design, we consider two architectural variants: the *Ent* design corresponds to the right-hand configuration illustrated in Figure 3, whereas the *Cyc* design follows the left-hand configuration in the same figure.

TABLE I
QNN BASELINE CONFIGS

VQC config	1	2	3	4	5	6	7	8	9	10	11	12
Component	Y	Y	Y	Y	Y	Y	N	N	N	N	N	N
Hadamard Gate	Y	Y	Y	Y	Y	Y	N	N	N	N	N	N
Entanglement	Ent	Ent	Ent	Cyc	Cyc	Cyc	Ent	Ent	Ent	Cyc	Cyc	Cyc
Rotation	R_x	R_y	R_z	R_x	R_y	R_z	R_x	R_y	R_z	R_x	R_y	R_z

A. Classification

1) *Simulation Setting*: For the classification tasks, we consider three binary settings: MNIST (digits 1 vs 5), FashionMNIST (classes 1 vs 5), and FashionMNIST (classes 5 vs 7). All models are trained using a batch size of 100 and the Adam optimizer with a learning rate of 10^{-3} . The QNN depth is set to 15 layers, as shallower circuits (i.e., with fewer than 15 layers) were found to be insufficient for successful training in preliminary experiments. In the conventional neural network setting, the total number of trainable parameters reaches 108,866. By contrast, the proposed DiffQAS-QT framework reduces this dramatically to only 286 trainable parameters, demonstrating the potential for substantial model compression while maintaining learnability.

2) *Result Analysis*: We conduct an initial evaluation of the proposed DiffQAS-QT approach on the MNIST dataset for binary classification between digits 1 and 5. As shown in Figure 5, DiffQAS-QT achieves performance close to the best manually-crafted QNN architectures, with slightly lower peak testing accuracy but significantly improved stability and generalization. The model exhibits smooth convergence with steadily decreasing loss and increasing accuracy, highlighting its robustness and efficiency despite being automatically discovered via differentiable architecture search. We further evaluate the proposed DiffQAS-QT framework on the FashionMNIST dataset for binary classification of classes 1 and 5. As shown in Figure 6, the DiffQAS-QT model achieves consistently strong performance, with training and testing accuracy exceeding 98% and comparable to the best manually-designed baselines. Although certain baseline configurations achieve faster initial convergence, the DiffQAS-QT model—automatically discovered via differentiable architecture optimization—demonstrates notable stability and low variance throughout training, especially in terms of testing accuracy. The model also maintains low training and testing loss throughout, indicating effective learning and strong generalization in more challenging visual domains. Finally, we assess the performance of DiffQAS-QT on the FashionMNIST dataset

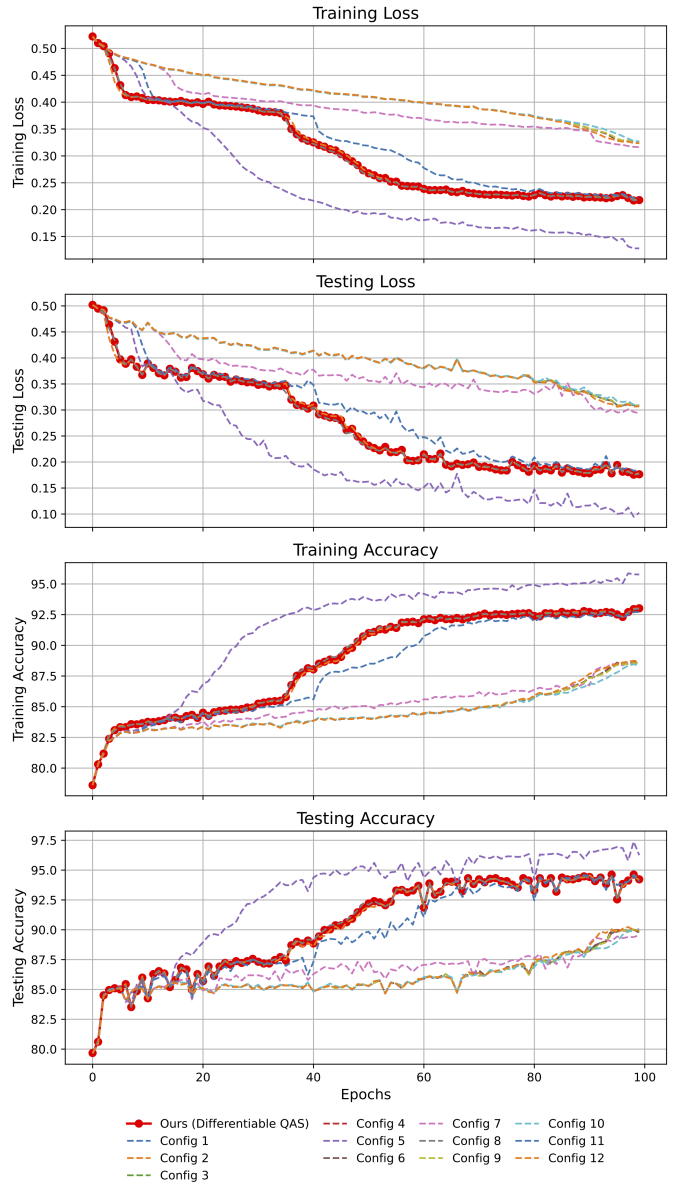


Fig. 5. Comparison of Various QNN Architectures on Binary Classification of Digits 1 and 5 from the MNIST Dataset.

for binary classification between labels 5 and 7, which are known to be visually similar and more challenging to separate. As illustrated in Figure 7, the proposed model consistently outperforms most baseline configurations in both training and testing accuracy. While several baselines exhibit early rapid gains, DiffQAS-QT achieves higher final accuracy with lower testing loss and smoother convergence. These results highlight the ability of the automatically discovered architecture to generalize effectively even in fine-grained classification scenarios.

B. Time-Series Prediction

1) *Simulation Setting*: For the time-series prediction tasks, we evaluate the DiffQAS-QT framework on five representative

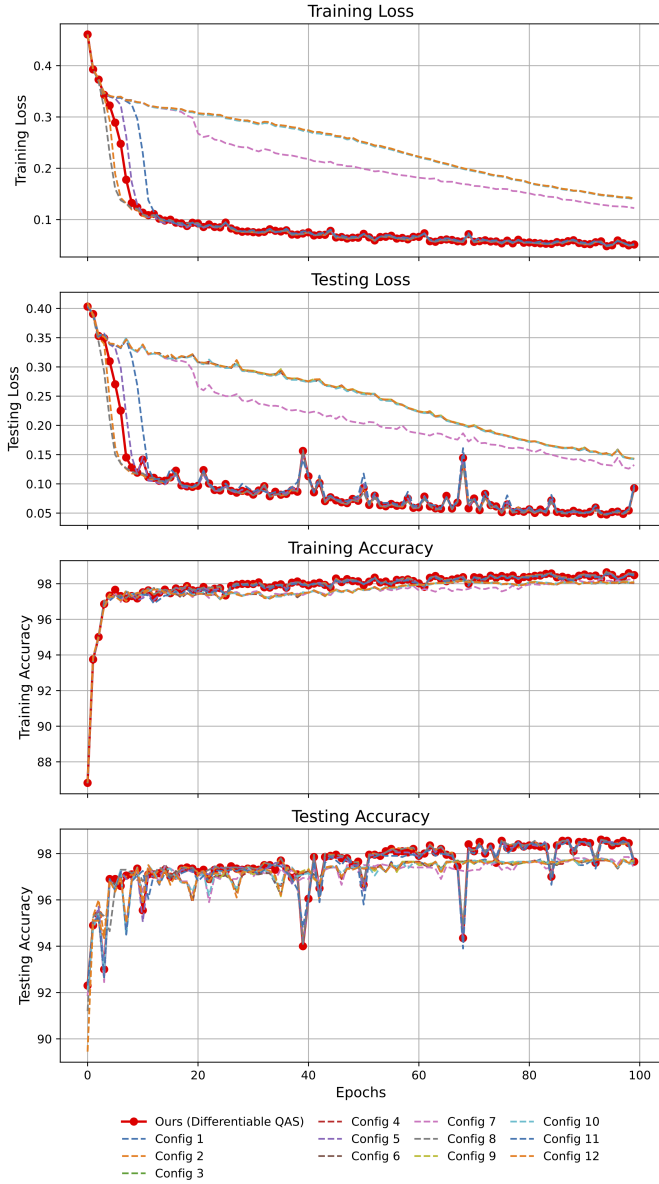


Fig. 6. Comparison of QNN Architectures on FashionMNIST Binary Classification (Labels 1 vs 5).

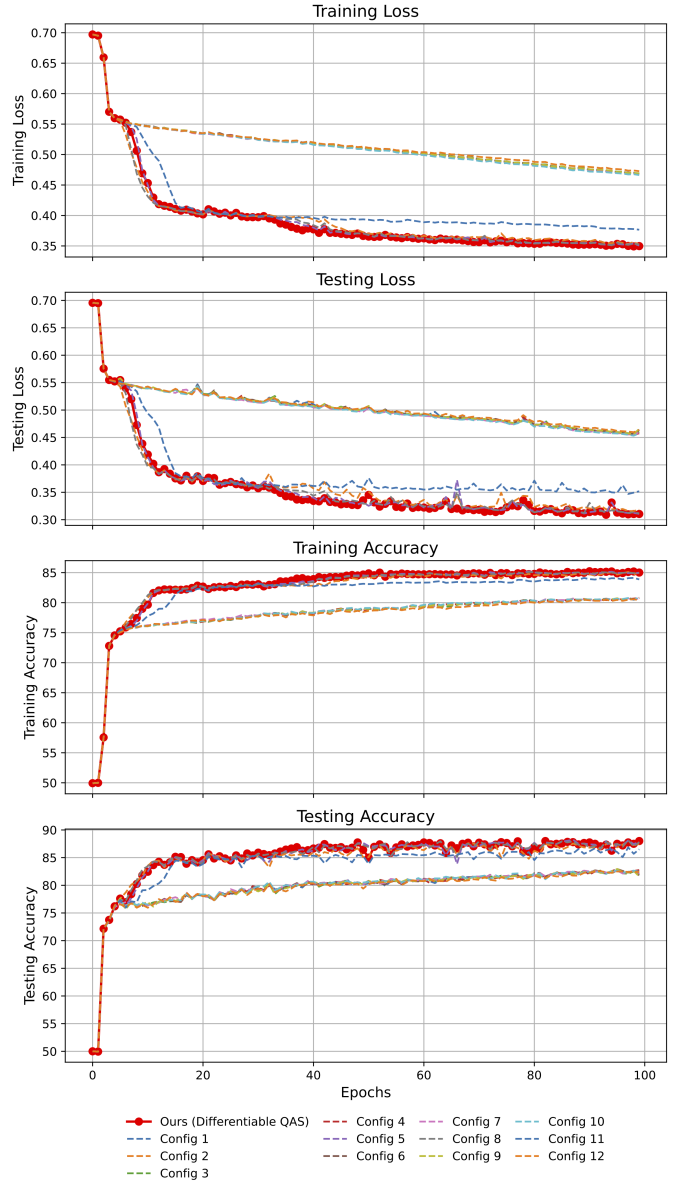


Fig. 7. Comparison of QNN Architectures on FashionMNIST Binary Classification (Labels 5 vs 7).

problems: the Bessel function J_2 , damped simple harmonic motion (SHM), delayed quantum control, and nonlinear autoregressive moving average models NARMA-5 and NARMA-10. In this setup, the DiffQAS-QT module is used to generate the parameters of an LSTM network. Training is conducted using a batch size of 10 and a QNN depth of 10. We adopt the RMSProp optimizer with a learning rate of 0.01, decay factor (alpha) of 0.99, and epsilon set to 10^{-8} . The conventional LSTM baseline contains 1,781 trainable parameters, while the DiffQAS-QT-based version reduces this to just 135, illustrating the framework’s ability to achieve efficient parameterization with minimal resource overhead. To prepare the dataset, we employ a sliding window strategy. Each input sequence is

composed of four consecutive values $[x_{t-4}, x_{t-3}, x_{t-2}, x_{t-1}]$, and the model is trained to predict the next value x_t . This window length is consistent with prior settings used in our QLSTM experiments [29], providing a coherent basis for comparison.

2) *Result Analysis*: We further evaluate the learned model in a time-series prediction task using the Bessel function (J_2) as the target signal. As shown in Figure 8, we visualize the model’s predictions at four representative training epochs: 1, 15, 30, and 100. The red dashed line marks the boundary between the training region (left) and the testing region (right). As training progresses, the model exhibits increasingly accurate prediction behavior, with tighter alignment to the

ground truth (orange dashed line) beyond the training horizon. By epoch 100, the prediction closely follows the ground truth across both the training and testing regions, indicating strong learning of the underlying temporal dynamics. We

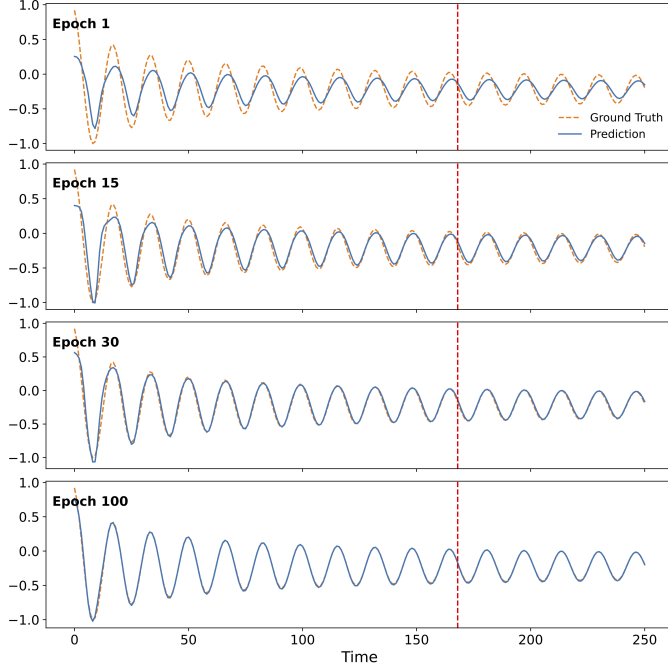


Fig. 8. **Model Rollout on Bessel Function at Different Training Epochs.** The red dashed line separates the training region (left) from the testing region (right). The model’s prediction (blue) improves over time in approximating the ground truth (orange), with increasing alignment beyond the training horizon from epoch 1 to epoch 100.

further evaluate the model on a time-series prediction task using a damped simple harmonic motion (Damped SHM) signal. As shown in Figure 9, the model is trained directly on this sequence and evaluated at four representative training epochs: 1, 15, 30, and 100. The red dashed line separates the training region from the testing region. Over time, the model learns to accurately capture the decaying oscillatory pattern, with prediction trajectories (blue) aligning closely with the ground truth (orange dashed line) by epoch 100. These results indicate the model’s ability to effectively learn and predict time-series signals with smooth, damped periodic structures. We further evaluate the model on a time-series prediction task inspired by delayed quantum control. The underlying physical system consists of a two-level atom (qubit) coupled to a semi-infinite one-dimensional waveguide terminated by a perfect mirror. The mirror induces complete reflection of propagating photons, creating delayed quantum feedback. When the qubit–mirror separation L is an integer multiple of the qubit’s resonant wavelength λ_0 , a bound state in the continuum (BIC) forms, resulting in persistent photon trapping between the qubit and the mirror [63]–[65]. In this setting, we consider a sinusoidal modulation of the qubit frequency such that its time-averaged value satisfies the resonance condition. This periodic detuning causes the intermittent release of the trapped photon

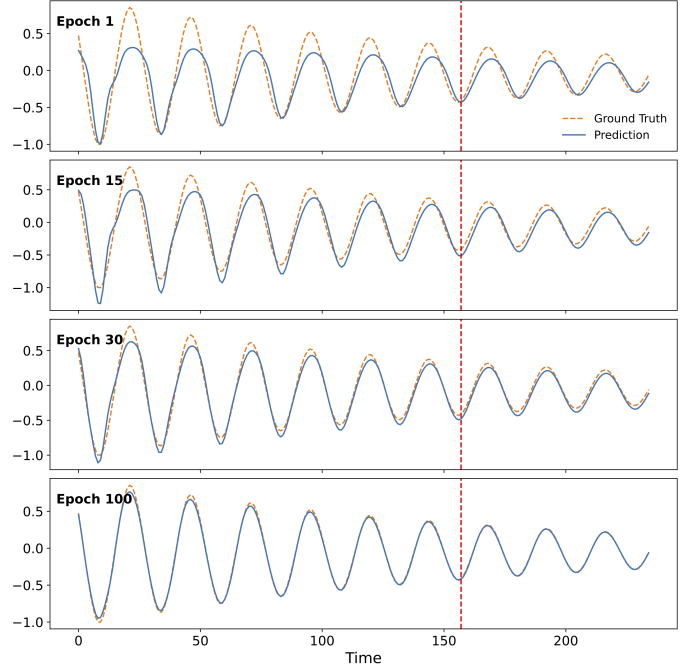


Fig. 9. **Model Rollout on Damped SHM at Different Training Epochs.** Same model architectures and training epochs as in the previous figure, trained and evaluated on a different time series.

population, producing a measurable, temporally structured emission pattern [64]. As shown in Figure 10, the model is trained to learn this non-Markovian quantum behavior [64], [66], [67] directly from the output field intensity. Across training epochs 1, 15, 30, and 100, the predicted output (blue) aligns increasingly well with the ground truth signal (orange dashed), including accurate reproduction of both emission timing and amplitude. By epoch 100, the model exhibits high-fidelity prediction over the testing region, indicating successful learning of the underlying delayed feedback dynamics. We further evaluate the model’s ability to capture nonlinear temporal dependencies using the NARMA benchmark tasks. Specifically, we consider both the NARMA 5 and NARMA 10 systems, which introduce increasing levels of long-range memory and nonlinear interactions between input and output sequences. As shown in Figure 11 and Figure 12, the model is trained on each system independently and evaluated at multiple training epochs. In both cases, the predicted output (blue) exhibits consistent improvement in the testing region over time, gradually aligning with the ground truth (orange dashed). While NARMA 10 poses a greater challenge due to its longer memory horizon and more complex dynamics, the model demonstrates stable prediction behavior and improved fidelity by epoch 100. These results highlight the model’s ability to handle nonlinear dynamics with varying degrees of temporal complexity. To quantitatively assess the model’s performance across diverse temporal tasks, we report the mean squared error (MSE) on five representative time-series datasets in Table II. The proposed DiffQAS-based QT-LSTM model

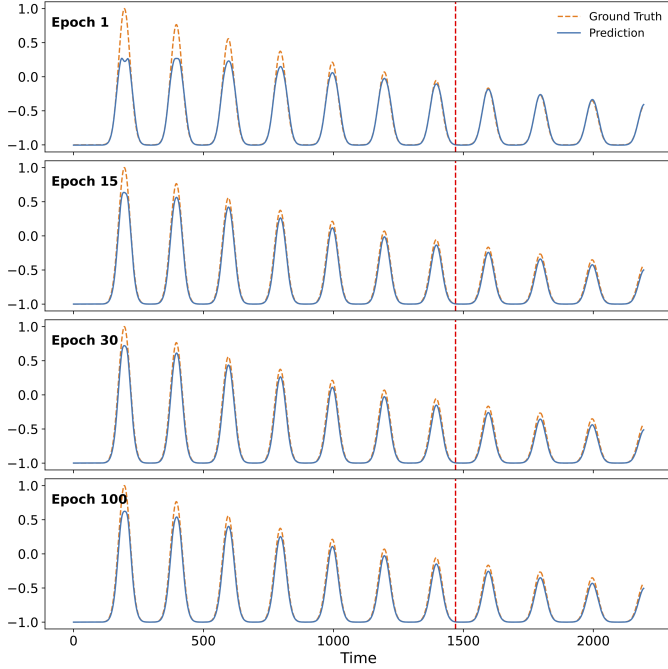


Fig. 10. **Model Rollout on Delayed Quantum Control at Different Training Epochs.** Same configuration, different time series instance.

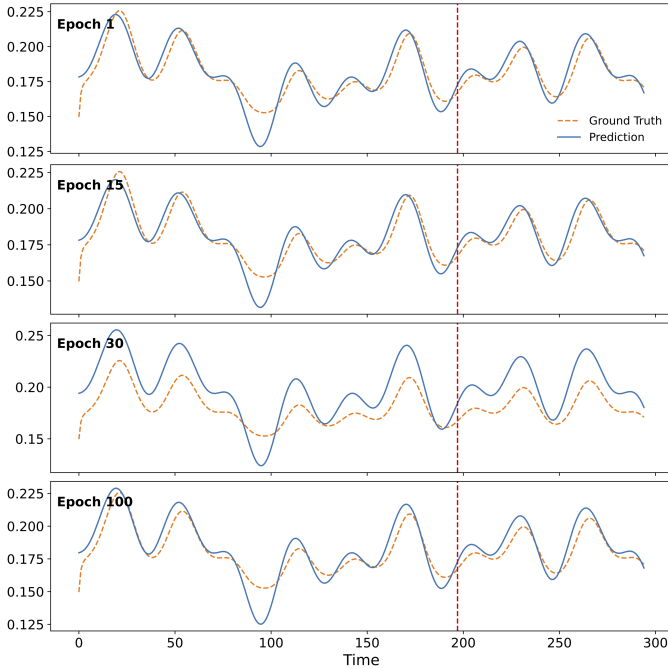


Fig. 11. **Model Rollout on NARMA 5 at Different Training Epochs.** Another test sequence; consistent improvement in testing region.

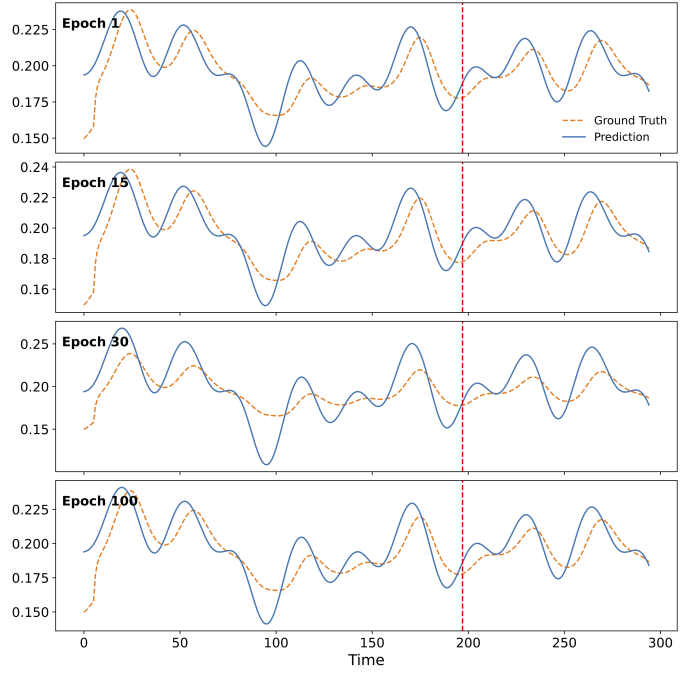


Fig. 12. **Model Rollout on NARMA 10 at Different Training Epochs.** Model exhibits stable learning and prediction across varied sequences.

consistently achieves competitive or superior performance across all benchmarks. It obtains the lowest MSE on the Bessel and damped SHM datasets, and remains within the top-performing group on delayed quantum control and both NARMA tasks. Notably, while some baseline configurations attain slightly lower error on specific tasks (e.g., Config 5 on NARMA 5, Config 8 on NARMA 10), they often fail to generalize across other datasets. In contrast, the proposed method demonstrates stable and robust performance under varied temporal dynamics, ranging from smooth decay and oscillations to non-Markovian quantum feedback and high-order autoregressive dependencies.

TABLE II
MULTI-TASK MSE COMPARISON ACROSS TIME-SERIES DATASETS

Model	Bessel ↓	Damped SHM ↓	Delayed QC ↓	NARMA 5 ↓	NARMA 10 ↓
Ours	0.000040	0.000036	0.001710	0.000050	0.000117
Config 1	0.000515	0.000155	0.000715	0.000038	0.000095
Config 2	0.000525	0.000695	0.001190	0.000068	0.000103
Config 3	0.000515	0.000155	0.000676	0.000038	0.000095
Config 4	0.000515	0.000155	0.002011	0.000038	0.000095
Config 5	0.002902	0.000820	0.001111	0.000024	0.000098
Config 6	0.000515	0.000155	0.002638	0.000038	0.000095
Config 7	0.000601	0.000040	0.001679	0.000052	0.000120
Config 8	0.000141	0.008873	0.001723	0.000091	0.000081
Config 9	0.001391	0.000154	0.000956	0.000045	0.000125
Config 10	0.000216	0.000157	0.001839	0.000040	0.000121
Config 11	0.007428	0.032072	0.000211	0.000054	0.000140
Config 12	0.001391	0.000154	0.000956	0.000045	0.000125

C. Reinforcement Learning

1) *Simulation Setting:* We further evaluate the DiffQAS-QT framework in the reinforcement learning (RL) setting using the MiniGrid-Empty environments of size 5×5 and 6×6

[68]. Training is conducted using the Asynchronous Advantage Actor-Critic (A3C) algorithm [26], [69], with 16 parallel worker processes. The discount factor is set to $\gamma = 0.9$, and model updates occur every 5 steps. For the quantum modules, we set the QNN depth to 10 and use the Adam optimizer with a learning rate of 10^{-4} and betas (0.92, 0.999). In the standard baseline configuration, the policy network and value network contain 6,023 and 5,825 trainable parameters, respectively. In contrast, under the DiffQAS-QT framework, each network incorporates its own DiffQAS-QT module comprising only 157 trainable parameters. This results in a combined total of just 314 parameters across both networks, highlighting a substantial reduction in model complexity.

2) *Result Analysis:* We evaluate the proposed DiffQAS-QT-RL model in a reinforcement learning setting using the MiniGrid-Empty-5x5 environment. Figure 13 shows the episodic rewards (moving average \pm standard deviation, window = 1000) across 50,000 episodes, compared to 12 manually-designed QNN baselines. The proposed model (black curve) achieves higher average rewards and significantly lower variance during the final training phase. The inset highlights the last 5,000 episodes, where our method consistently outperforms most baselines in both performance and stability. These results suggest that the differentiable quantum architecture search framework can effectively discover robust quantum-enhanced policies for navigation tasks in grid-based environments. To assess the robustness of our method under increased spatial complexity, we further evaluate it on the MiniGrid-Empty-6x6 environment. As shown in Figure 14, the reward learning curves maintain trends consistent with the 5x5 case. The DiffQAS-QT-RL model continues to outperform most handcrafted baselines in both final reward and stability, especially during the late-stage episodes as highlighted in the zoomed-in inset. These results suggest that our architecture search framework is capable of discovering quantum-enhanced policies that scale well with task complexity, retaining strong performance under more demanding exploration and navigation conditions.

VII. CONCLUSION AND FUTURE WORK

This paper demonstrates the effectiveness of applying differentiable quantum architecture search (DiffQAS) for constructing quantum-enhanced neural network programmer, referred to as quantum-train (QT), across three fundamental learning paradigms—supervised classification, time-series prediction, and reinforcement learning. Our results show that QNN architectures discovered via DiffQAS not only achieve performance competitive with or superior to handcrafted baselines, but also generalize well across tasks with varying temporal and spatial complexity. The broad applicability of DiffQAS-QT across supervised, temporal, and interactive settings suggests that differentiable quantum architecture search may serve as a core engine for developing versatile, high-performing quantum AI systems.

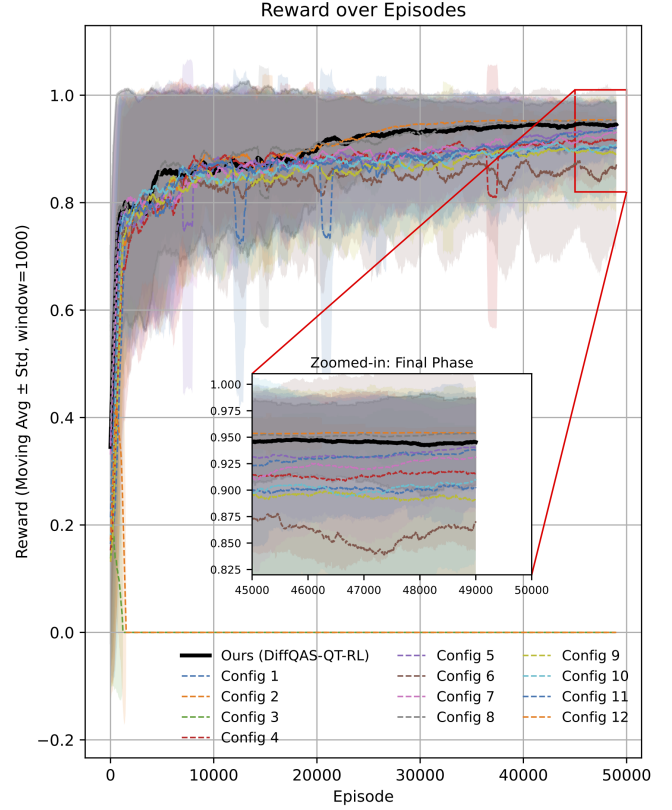


Fig. 13. **Reward Curve Comparison on MiniGrid-Empty-5x5 Environment.** Episodic rewards (moving average \pm standard deviation, window = 1000) over 50,000 episodes are shown for our method (DiffQAS-QT-RL, black) and 12 manually-designed baseline configurations. The red inset zooms into the final 5,000 episodes, where our method consistently demonstrates higher rewards and greater stability compared to most baselines.

ACKNOWLEDGMENT

Wei-Hao Huang (Jij inc) acknowledges this work was performed for the Council for Science, Technology and Innovation (CSTI), Cross-ministerial Strategic Innovation Promotion Program (SIP), “Promoting the application of advanced quantum technology platforms to social issues” (Funding agency: QST). This work was supported by the Engineering and Physical Sciences Research Council (EPSRC) under grant number EP/W032643/1.

REFERENCES

- [1] J. Biamonte, P. Wittek, N. Pancotti, P. Rebentrost, N. Wiebe, and S. Lloyd, “Quantum machine learning,” *Nature*, vol. 549, no. 7671, pp. 195–202, 2017.
- [2] V. Dunjko, J. M. Taylor, and H. J. Briegel, “Quantum-enhanced machine learning,” *Physical review letters*, vol. 117, no. 13, p. 130501, 2016.
- [3] M. Cerezo, A. Arrasmith, R. Babbush, S. C. Benjamin, S. Endo, K. Fujii, J. R. McClean, K. Mitarai, X. Yuan, L. Cincio *et al.*, “Variational quantum algorithms,” *Nature Reviews Physics*, vol. 3, no. 9, pp. 625–644, 2021.
- [4] K. Bharti, A. Cervera-Lierta, T. H. Kyaw, T. Haug, S. Alperin-Lea, A. Anand, M. Degroote, H. Heimonen, J. S. Kottmann, T. Menke *et al.*, “Noisy intermediate-scale quantum algorithms,” *Reviews of Modern Physics*, vol. 94, no. 1, p. 015004, 2022.

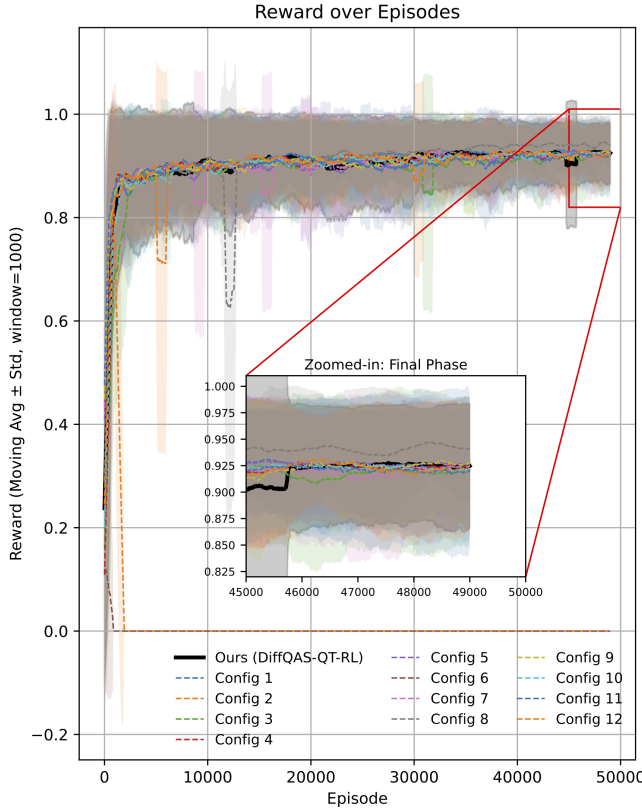


Fig. 14. **Reward Curve Comparison on MiniGrid-Empty-6x6 Environment.** Results on the larger 6x6 environment show trends consistent with the 5x5 case. Our method (DiffQAS-QT-RL) maintains superior reward and stability over most handcrafted baselines, indicating robustness to increased spatial complexity.

- [5] A. Abbas, D. Sutter, C. Zoufal, A. Lucchi, A. Figalli, and S. Woerner, "The power of quantum neural networks," *Nature Computational Science*, vol. 1, no. 6, pp. 403–409, 2021.
- [6] Y. Du, M.-H. Hsieh, T. Liu, and D. Tao, "Expressive power of parametrized quantum circuits," *Physical Review Research*, vol. 2, no. 3, p. 033125, 2020.
- [7] M. C. Caro, H.-Y. Huang, M. Cerezo, K. Sharma, A. Sornborger, L. Cincio, and P. J. Coles, "Generalization in quantum machine learning from few training data," *Nature communications*, vol. 13, no. 1, pp. 1–11, 2022.
- [8] K.-C. Chen, T.-Y. Li, Y.-Y. Wang, S. See, C.-C. Wang, R. Wille, N.-Y. Chen, A.-C. Yang, and C.-Y. Lin, "Validating large-scale quantum machine learning: Efficient simulation of quantum support vector machines using tensor networks," *Machine Learning: Science and Technology*, 2024.
- [9] K. Mitarai, M. Negoro, M. Kitagawa, and K. Fujii, "Quantum circuit learning," *Physical Review A*, vol. 98, no. 3, p. 032309, 2018.
- [10] S. Y.-C. Chen, C.-M. Huang, C.-W. Hsing, and Y.-J. Kao, "An end-to-end trainable hybrid classical-quantum classifier," *Machine Learning: Science and Technology*, vol. 2, no. 4, p. 045021, 2021.
- [11] S. Y.-C. Chen, T.-C. Wei, C. Zhang, H. Yu, and S. Yoo, "Quantum convolutional neural networks for high energy physics data analysis," *Physical Review Research*, vol. 4, no. 1, p. 013231, 2022.
- [12] K.-C. Chen, X. Xu, H. Makhanov, H.-H. Chung, and C.-Y. Liu, "Quantum-enhanced support vector machine for large-scale multi-class stellar classification," in *International Conference on Intelligent Computing*. Springer, 2024, pp. 155–168.
- [13] K.-C. Chen, Y.-T. Li, T.-Y. Li, and C.-Y. Liu, "Compressedmediq: Hybrid quantum machine learning pipeline for high-dimensional neuroimaging data," *arXiv preprint arXiv:2409.08584*, 2024.
- [14] C.-S. Chen, S. Y.-C. Chen, A. H.-W. Tsai, and C.-S. Wei, "Qeeqnet: Quantum machine learning for enhanced electroencephalography encoding," in *2024 IEEE Workshop on Signal Processing Systems (SiPS)*. IEEE, 2024, pp. 153–158.
- [15] H.-Y. Lin, H.-H. Tseng, S. Y.-C. Chen, and S. Yoo, "Quantum gradient class activation map for model interpretability," in *2024 IEEE Workshop on Signal Processing Systems (SiPS)*. IEEE, 2024, pp. 165–170.
- [16] H.-H. Tseng, H.-Y. Lin, S. Y.-C. Chen, and S. Yoo, "Transfer learning analysis of variational quantum circuits," *arXiv preprint arXiv:2501.01507*, 2025.
- [17] J. Qi, C.-H. Yang, and P.-Y. Chen, "Qtn-vqc: An end-to-end learning framework for quantum neural networks," *Physica Scripta*, vol. 99, no. 1, p. 015111, 2023.
- [18] S. Y.-C. Chen, C.-H. H. Yang, J. Qi, P.-Y. Chen, X. Ma, and H.-S. Goan, "Variational quantum circuits for deep reinforcement learning," *IEEE access*, vol. 8, pp. 141 007–141 024, 2020.
- [19] S. Y.-C. Chen, C.-M. Huang, C.-W. Hsing, H.-S. Goan, and Y.-J. Kao, "Variational quantum reinforcement learning via evolutionary optimization," *Machine Learning: Science and Technology*, vol. 3, no. 1, p. 015025, 2022.
- [20] W. J. Yun, J. Park, and J. Kim, "Quantum multi-agent meta reinforcement learning," in *Proceedings of the AAAI Conference on Artificial Intelligence*, vol. 37, no. 9, 2023, pp. 11 087–11 095.
- [21] S. Y.-C. Chen, "Efficient quantum recurrent reinforcement learning via quantum reservoir computing," in *ICASSP 2024-2024 IEEE International Conference on Acoustics, Speech and Signal Processing (ICASSP)*. IEEE, 2024, pp. 13 186–13 190.
- [22] O. Lockwood and M. Si, "Reinforcement learning with quantum variational circuit," in *Proceedings of the AAAI conference on artificial intelligence and interactive digital entertainment*, vol. 16, no. 1, 2020, pp. 245–251.
- [23] A. Skolik, S. Jerbi, and V. Dunjko, "Quantum agents in the gym: a variational quantum algorithm for deep q-learning," *Quantum*, vol. 6, p. 720, 2022.
- [24] S. Jerbi, C. Gyurik, S. Marshall, H. Briegel, and V. Dunjko, "Parametrized quantum policies for reinforcement learning," *Advances in Neural Information Processing Systems*, vol. 34, pp. 28 362–28 375, 2021.
- [25] S. Y.-C. Chen, "Quantum deep recurrent reinforcement learning," in *ICASSP 2023-2023 IEEE International Conference on Acoustics, Speech and Signal Processing (ICASSP)*. IEEE, 2023, pp. 1–5.
- [26] —, "Asynchronous training of quantum reinforcement learning," *Procedia Computer Science*, vol. 222, pp. 321–330, 2023.
- [27] —, "Quantum deep q-learning with distributed prioritized experience replay," in *2023 IEEE International Conference on Quantum Computing and Engineering (QCE)*, vol. 2. IEEE, 2023, pp. 31–35.
- [28] —, "Learning to program variational quantum circuits with fast weights," in *2024 International Joint Conference on Neural Networks (IJCNN)*. IEEE, 2024, pp. 1–9.
- [29] S. Y.-C. Chen, S. Yoo, and Y.-L. L. Fang, "Quantum long short-term memory," in *ICASSP 2022-2022 IEEE International Conference on Acoustics, Speech and Signal Processing (ICASSP)*. IEEE, 2022, pp. 8622–8626.
- [30] S. Y.-C. Chen, D. Fry, A. Deshmukh, V. Rastunkov, and C. Stefanski, "Reservoir computing via quantum recurrent neural networks," *arXiv preprint arXiv:2211.02612*, 2022.
- [31] C.-H. A. Lin, C.-Y. Liu, and K.-C. Chen, "Quantum-train long short-term memory: Application on flood prediction problem," in *2024 IEEE International Conference on Quantum Computing and Engineering (QCE)*, vol. 2. IEEE, 2024, pp. 268–273.
- [32] M. Chehimi, S. Y.-C. Chen, W. Saad, and S. Yoo, "Federated quantum long short-term memory (fedqlstm)," *Quantum Machine Intelligence*, vol. 6, no. 2, p. 43, 2024.
- [33] C.-H. H. Yang, J. Qi, S. Y.-C. Chen, P.-Y. Chen, S. M. Siniscalchi, X. Ma, and C.-H. Lee, "Decentralizing feature extraction with quantum convolutional neural network for automatic speech recognition," in *ICASSP 2021-2021 IEEE International Conference on Acoustics, Speech and Signal Processing (ICASSP)*. IEEE, 2021, pp. 6523–6527.
- [34] C.-H. H. Yang, J. Qi, S. Y.-C. Chen, Y. Tsao, and P.-Y. Chen, "When bert meets quantum temporal convolution learning for text classification in heterogeneous computing," in *ICASSP 2022-2022 IEEE International Conference on Acoustics, Speech and Signal Processing (ICASSP)*. IEEE, 2022, pp. 8602–8606.

- [35] R. Di Sipio, J.-H. Huang, S. Y.-C. Chen, S. Mangini, and M. Worring, "The dawn of quantum natural language processing," in *ICASSP 2022-2022 IEEE International Conference on Acoustics, Speech and Signal Processing (ICASSP)*. IEEE, 2022, pp. 8612–8616.
- [36] J. Stein, I. Christ, N. Kraus, M. B. Mansky, R. Müller, and C. Linnhoff-Popien, "Applying qnlp to sentiment analysis in finance," in *2023 IEEE International Conference on Quantum Computing and Engineering (QCE)*, vol. 2. IEEE, 2023, pp. 20–25.
- [37] S. S. Li, X. Zhang, S. Zhou, H. Shu, R. Liang, H. Liu, and L. P. Garcia, "Pqim-multilingual decentralized portable quantum language model," in *ICASSP 2023-2023 IEEE International Conference on Acoustics, Speech and Signal Processing (ICASSP)*. IEEE, 2023, pp. 1–5.
- [38] C.-Y. Liu, E.-J. Kuo, C.-H. A. Lin, S. Chen, J. G. Young, Y.-J. Chang, and M.-H. Hsieh, "Training classical neural networks by quantum machine learning," in *2024 IEEE International Conference on Quantum Computing and Engineering (QCE)*, vol. 2. IEEE, 2024, pp. 34–38.
- [39] C.-Y. Liu, E.-J. Kuo, C.-H. A. Lin, J. G. Young, Y.-J. Chang, M.-H. Hsieh, and H.-S. Goan, "Quantum-train: Rethinking hybrid quantum-classical machine learning in the model compression perspective," *arXiv preprint arXiv:2405.11304*, 2024.
- [40] C.-Y. Liu, C.-H. A. Lin, C.-H. H. Yang, K.-C. Chen, and M.-H. Hsieh, "Qtrl: Toward practical quantum reinforcement learning via quantum-train," in *2024 IEEE International Conference on Quantum Computing and Engineering (QCE)*, vol. 2. IEEE, 2024, pp. 317–322.
- [41] C.-Y. Liu and S. Y.-C. Chen, "Federated quantum-train with batched parameter generation," in *2024 15th International Conference on Information and Communication Technology Convergence (ICTC)*. IEEE, 2024, pp. 1133–1138.
- [42] C.-Y. Liu, C.-H. A. Lin, and K.-C. Chen, "Quantum-train with tensor network mapping model and distributed circuit ansatz," in *ICASSP 2025-2025 IEEE International Conference on Acoustics, Speech and Signal Processing (ICASSP)*. IEEE, 2025, pp. 1–4.
- [43] C.-H. A. Lin, C.-Y. Liu, S. Y.-C. Chen, and K.-C. Chen, "Quantum-trained convolutional neural network for deepfake audio detection," *arXiv preprint arXiv:2410.09250*, 2024.
- [44] C.-Y. Liu, C.-H. H. Yang, H.-S. Goan, and M.-H. Hsieh, "A quantum circuit-based compression perspective for parameter-efficient learning," in *The Thirteenth International Conference on Learning Representations*, 2025.
- [45] C.-Y. Liu, S. Y.-C. Chen, K.-C. Chen, W.-J. Huang, and Y.-J. Chang, "Federated quantum-train long short-term memory for gravitational wave signal," *arXiv preprint arXiv:2503.16049*, 2025.
- [46] K.-C. Chen, S. Y.-C. Chen, C.-Y. Liu, and K. K. Leung, "Quantum-train-based distributed multi-agent reinforcement learning," *arXiv preprint arXiv:2412.08845*, 2024.
- [47] C.-Y. Liu, S. Y.-C. Chen, K.-C. Chen, W.-J. Huang, and Y.-J. Chang, "Programming variational quantum circuits with quantum-train agent," *arXiv preprint arXiv:2412.01173*, 2024.
- [48] C.-Y. Liu, C.-H. A. Lin, W.-J. Huang, and M.-H. Hsieh, "Introduction to quantum-train toolkit," in *2024 IEEE International Conference on Quantum Computing and Engineering (QCE)*, vol. 2. IEEE, 2024, pp. 456–457.
- [49] C.-Y. Liu, K.-C. Chen, S. Y.-C. Chen, H. wei hao, W.-J. Huang, and Y. J. Chang, "Frame generation in hilbert space: Generative interpolation of measurement data for quantum parameter adaptation," in *ICLR 2025 Workshop on Deep Generative Model in Machine Learning: Theory, Principle and Efficacy*, 2025.
- [50] D. Martyniuk, J. Jung, and A. Paschke, "Quantum architecture search: a survey," in *2024 IEEE International Conference on Quantum Computing and Engineering (QCE)*, vol. 1. IEEE, 2024, pp. 1695–1706.
- [51] E.-J. Kuo, Y.-L. L. Fang, and S. Y.-C. Chen, "Quantum architecture search via deep reinforcement learning," *arXiv preprint arXiv:2104.07715*, 2021.
- [52] E. Ye and S. Y.-C. Chen, "Quantum architecture search via continual reinforcement learning," *arXiv preprint arXiv:2112.05779*, 2021.
- [53] S. Y.-C. Chen, "Quantum reinforcement learning for quantum architecture search," in *Proceedings of the 2023 international workshop on quantum classical cooperative*, 2023, pp. 17–20.
- [54] X. Dai, T.-C. Wei, S. Yoo, and S. Y.-C. Chen, "Quantum machine learning architecture search via deep reinforcement learning," in *2024 IEEE International Conference on Quantum Computing and Engineering (QCE)*, vol. 1. IEEE, 2024, pp. 1525–1534.
- [55] L. Ding and L. Spector, "Evolutionary quantum architecture search for parametrized quantum circuits," in *Proceedings of the Genetic and Evolutionary Computation Conference Companion*, 2022, pp. 2190–2195.
- [56] S. Y.-C. Chen, "Evolutionary optimization for designing variational quantum circuits with high model capacity," *arXiv preprint arXiv:2412.12484*, 2024.
- [57] H. Liu, K. Simonyan, and Y. Yang, "Darts: Differentiable architecture search," *arXiv preprint arXiv:1806.09055*, 2018.
- [58] S.-X. Zhang, C.-Y. Hsieh, S. Zhang, and H. Yao, "Differentiable quantum architecture search," *Quantum Science and Technology*, vol. 7, no. 4, p. 045023, 2022.
- [59] Y. Sun, Y. Ma, and V. Tresp, "Differentiable quantum architecture search for quantum reinforcement learning," in *2023 IEEE International Conference on Quantum Computing and Engineering (QCE)*, vol. 2. IEEE, 2023, pp. 15–19.
- [60] S. Y.-C. Chen, "Differentiable quantum architecture search in asynchronous quantum reinforcement learning," in *2024 IEEE International Conference on Quantum Computing and Engineering (QCE)*, vol. 1. IEEE, 2024, pp. 1516–1524.
- [61] S. Y.-C. Chen, H.-H. Tseng, H.-Y. Lin, and S. Yoo, "Learning to measure quantum neural networks," *arXiv preprint arXiv:2501.05663*, 2025.
- [62] S. Sim, P. D. Johnson, and A. Aspuru-Guzik, "Expressibility and entangling capability of parameterized quantum circuits for hybrid quantum-classical algorithms," *Advanced Quantum Technologies*, vol. 2, no. 12, p. 1900070, 2019.
- [63] G. Calajó, Y.-L. L. Fang, H. U. Baranger, and F. Ciccarello, "Exciting a bound state in the continuum through multiphoton scattering plus delayed quantum feedback," *Physical review letters*, vol. 122, no. 7, p. 073601, 2019.
- [64] T. Tufarelli, F. Ciccarello, and M. Kim, "Dynamics of spontaneous emission in a single-end photonic waveguide," *Physical Review A—Atomic, Molecular, and Optical Physics*, vol. 87, no. 1, p. 013820, 2013.
- [65] H. Dong, Z. Gong, H. Ian, L. Zhou, and C. Sun, "Intrinsic cavity qed and emergent quasinormal modes for a single photon," *Physical Review A—Atomic, Molecular, and Optical Physics*, vol. 79, no. 6, p. 063847, 2009.
- [66] T. Tufarelli, M. Kim, and F. Ciccarello, "Non-markovianity of a quantum emitter in front of a mirror," *Physical Review A*, vol. 90, no. 1, p. 012113, 2014.
- [67] Y.-L. L. Fang, F. Ciccarello, and H. U. Baranger, "Non-markovian dynamics of a qubit due to single-photon scattering in a waveguide," *New Journal of Physics*, vol. 20, no. 4, p. 043035, 2018.
- [68] M. Chevalier-Boisvert, L. Willems, and S. Pal, "Minimalistic grid-world environment for openai gym," <https://github.com/maximecb/gym-minigrid>, 2018.
- [69] V. Mnih, A. P. Badia, M. Mirza, A. Graves, T. Lillicrap, T. Harley, D. Silver, and K. Kavukcuoglu, "Asynchronous methods for deep reinforcement learning," in *International conference on machine learning*. PMLR, 2016, pp. 1928–1937.